Corrosion Inhibition Performance of Waterborne Acrylic Copolymer Nanoparticles: Experimental and Theoretical Insights into Copolymer Composition

Mohammad Samiei, Golamali Farzi *, Zeinab Jarrahi

Department of Polymer Engineering, Faculty of Petroleum and Petrochemical Engineering, Hakim Sabzevari University, Sabzevar, Iran

Editor's note: The development of waterborne corrosion inhibitors has become a promising strategy to protect metallic materials from degradation in aggressive environments while minimizing the use of volatile organic solvents. This study by Samiei et al. investigates methyl methacrylate–butyl acrylate (MMA-co-BuA) copolymers as waterborne corrosion inhibitors for mild steel in 1 M HCl. Synthesized via miniemulsion polymerization, these copolymers show increased corrosion protection with higher MMA content, achieving an 82.7% inhibition efficiency at an 80:20 MMA:BuA ratio and 40 ppm. The reported enhanced performance is linked to improved polarity and interfacial interactions that strengthen the protective layer on the steel surface.

doi: 10.22034/jams.2026.260306

How to cite: M. Samiei et al., *Journal of Applied Material Science*, **2026**, *2*, 260306.

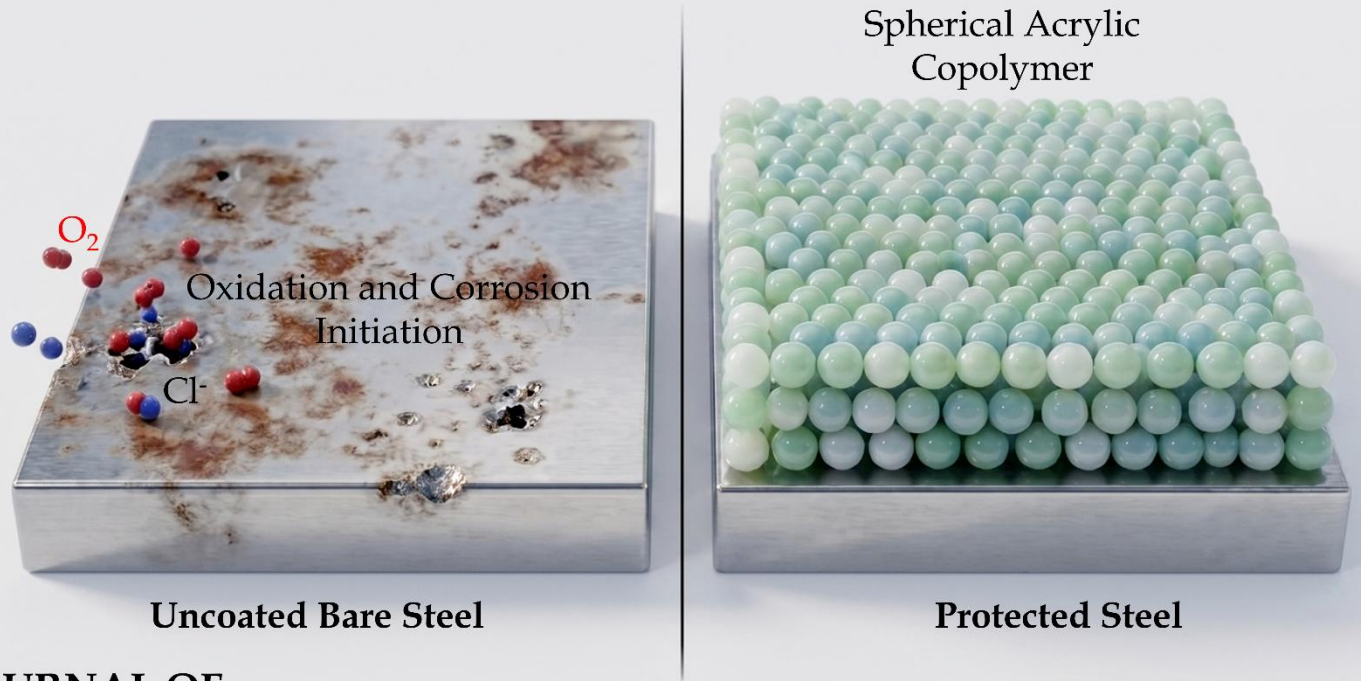

JOURNAL OF
APPLIED MATERIAL SCIENCE
jams.hsu.ac.ir

Journal of Applied Material Science **2026**, 2, 260306
How to cite: M. Samiei et al., *Journal of Applied Material Science*, **2026**, 2, 260306.
Journal homepage: **jams.hsu.ac.ir**

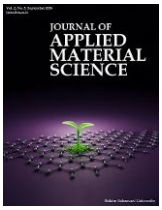

Original Research

Corrosion Inhibition Performance of Waterborne Acrylic Copolymer Nanoparticles: Experimental and Theoretical Insights into Copolymer Composition

Mohammad Samiei, Golamali Farzi *, Zeinab Jarrahi

Department of Polymer Engineering, Faculty of Petroleum and Petrochemical Engineering, Hakim Sabzevari University, Sabzevar, Iran

Abstract

The development of waterborne corrosion inhibitors has emerged as a promising strategy for mitigating the degradation of metallic materials in aggressive media while reducing the use of volatile organic solvents. In this context, acrylic copolymers synthesized via miniemulsion polymerization have demonstrated notable corrosion inhibition performance in various corrosive environments, including HCl, H_2SO_4, and NaCl solutions. In the present study, methyl methacrylate–butyl acrylate (MMA-co-BuA) copolymers with varying monomer composition were synthesized, and their corrosion inhibition behavior toward mild steel in 1 M HCl was systematically investigated. Electrochemical techniques, namely potentiodynamic polarization (PDP) and electrochemical impedance spectroscopy (EIS), were employed to evaluate the inhibition performance. The thermal stability and particle size distribution of the synthesized copolymers were examined using thermogravimetric analysis (TGA) and dynamic light scattering (DLS), respectively. Furthermore, the molecular structures, electronic properties, and reactivity of the copolymers were analyzed using quantum-chemical calculations based on density functional theory (DFT) and molecular dynamics (MD) simulations. The results indicate that increasing the MMA content enhances the corrosion inhibition performance of the MMA-co-BuA copolymer. This behavior may be related to variations in copolymer polarity and interfacial interactions, which could influence the adsorption process at the metal/electrolyte interface. Notably, at an MMA: BuA ratio of 80:20 and an inhibitor concentration of 40 ppm, a maximum inhibition efficiency of 82.7% was achieved. This enhanced performance may be associated with changes in copolymer polarity and interfacial interactions resulting from the increased MMA content, thereby promoting the formation of a more effective protective layer on the steel surface.

Keywords: Electrochemical impedance spectroscopy; Acrylic copolymer nanoparticles; Corrosion inhibitor; Miniemulsion polymerization; Molecular simulation.

* Corresponding author.
Email address: farzi@hsu.ac.ir (G. Farzi)

Received 26 June 2026
Revised 22 August 2026
Accepted 26 August 2026
Available online 07 September 2026

https://doi.org/10.22034/jams.2026.260306

1. Introduction

Due to its outstanding mechanical properties and relatively low production cost, carbon steel is widely employed across numerous industrial sectors. However, its extensive use is severely constrained by corrosion, an unavoidable and pervasive phenomenon that causes substantial economic and financial losses in engineering infrastructure. Consequently, assessing corrosion processes and developing effective mitigation strategies remain critical concerns within the scientific and engineering communities [1-5]. Among the various protection methods, corrosion inhibitors are commonly applied to reduce the rate of metal dissolution in aggressive environments. In recent decades, extensive research has focused on organic inhibitors containing heteroatoms such as sulfur, nitrogen, and oxygen, which are known to exhibit high inhibition efficiency against carbon steel in acidic media. Despite their effectiveness, the inherent toxicity and environmental concerns associated with these compounds have prompted increasing interest in alternative corrosion inhibitors with reduced environmental impact [6-11].

Recent studies have also highlighted the development of sustainable, environmentally friendly approaches to corrosion protection, including green inhibitors derived from natural extracts and protective composite coatings. For instance, plant-based extracts and electrodeposited composite coatings have demonstrated promising corrosion protection performance by forming protective barriers and reducing the interaction between corrosive species and metal surfaces [12-14].

In this regard, acrylic-based homopolymers and copolymers have attracted considerable attention as promising corrosion inhibitors for carbon steel in aggressive solutions, particularly in waterborne formulations with reduced VOC emissions compared with conventional solvent-based systems. Acrylic polymers possess functional groups with high electron density—particularly hydroxyl (–OH) and carboxyl (–COOH) groups—which can adsorb onto the metal surface and hinder the penetration of aggressive ions. Notably, the inhibition performance of such polymers is strongly influenced by the mechanical integrity, structural arrangement, and chemical composition of the protective layer formed during adsorption [15-20]. Recent studies have emphasized that polymeric corrosion inhibitors can provide enhanced protection through multiple adsorption interactions, including electrostatic attraction, coordination, and physical/chemical adsorption on metal surfaces. The formation of a stable polymeric film at the metal/electrolyte interface is considered a key factor governing their inhibition efficiency [21]. Various synthesis techniques have been employed to produce acrylic polymers, among which miniemulsion polymerization has emerged as a particularly effective approach. This technique, predominantly based on free-radical polymerization, enables the synthesis of a wide range of monomers, including acrylates, methacrylates, acrylamides, and styrenic derivatives. Moreover, copolymerization of monomers with different polarities, such as hydrophobic and relatively hydrophilic monomers, enables the formation of amphiphilic copolymers with tunable physicochemical properties, thereby facilitating the preparation of polymeric nanoparticles with controlled morphology and size [22-24].

Owing to their high surface-to-volume ratio and enhanced interfacial activity, polymeric nanoparticles have garnered significant interest as efficient alternatives to conventional corrosion inhibitors [25]. Recent advances in polymeric corrosion inhibitors have highlighted the critical role of polymer architecture, functional groups, and multiple adsorption sites in enhancing corrosion protection performance. Compared with conventional small-molecule inhibitors, polymeric systems can form more stable protective films via multidentate interactions with metal surfaces, thereby improving inhibition efficiency and durability [26]. Recent reviews have further highlighted the emerging challenges and prospects of polymeric corrosion inhibitors, particularly the importance of molecular design, adsorption mechanisms, and polymer architecture for achieving efficient corrosion control in aggressive environments [27]. In parallel, the combination of polymers with nanomaterials has been extensively explored to fabricate nanocomposites that serve as effective barriers against corrosive species. For instance, Yang et al. [28] synthesized uniform spherical polydopamine (PDA) nanoparticles via self-polymerization and demonstrated a corrosion inhibition efficiency of up to 86% in 1 M HCl, attributed to the strong adsorption capacity of PDA nanoparticles and the formation of a protective interfacial film. Similarly, Huang et al. [29] developed A-zirconium/polyurethane (ZrP/PU) nanocomposites. They reported enhanced

corrosion protection compared with pristine PU coatings, resulting from the barrier effect of zirconium-based nanostructures and reduced water penetration at the metal/electrolyte interface. In addition, polymers such as polyacrylic acid [30], polyaniline [31, 32], polyanthranilic acid [33], polyacrylamide [34], chitosan [35], and polyvinyl alcohol [36] have been extensively investigated as anticorrosive materials. Acrylic copolymers, in particular, are among the most widely used materials in waterborne coating systems. Recent studies have demonstrated that the molecular design of acrylic-based polymeric systems and incorporation of functional groups can significantly influence their corrosion protection performance [37]. Ji et al. [38] synthesized acrylic–alkyd copolymers via free-radical polymerization and reported a significant reduction in water diffusion coefficients alongside enhanced coating hydrophobicity, both of which contributed markedly to improved corrosion resistance. Recent studies have demonstrated that polymer architecture and functional group density strongly influence corrosion inhibition performance. Polymeric inhibitors with multiple adsorption sites can provide greater surface coverage and stronger interactions with metal substrates, thereby improving protective film formation. Verma et al. reported that aqueous-phase polymeric inhibitors exhibit strong adsorption on metallic surfaces due to their polymeric structure and polar functional groups, leading to effective corrosion protection [21]. Similarly, Wang et al. highlighted that polymer architecture, adsorption sites, and functional group distribution are critical parameters governing the inhibition performance of polymeric corrosion inhibitors [26]. In addition, Chen et al. demonstrated that a functionalized copolymer inhibitor provided improved corrosion protection through the synergistic effect of multiple adsorption centers and strong interfacial interactions with carbon steel [39].

Acrylic copolymers synthesized through miniemulsion polymerization represent a class of advanced materials with tunable physicochemical properties [32]. Miniemulsion polymerization involves the formation of stable submicron monomer droplets dispersed in an aqueous phase using surfactants and stabilizers, with polymerization initiated once the monomer concentration exceeds the critical micelle concentration (CMC). This approach enables precise control over particle size, composition, and morphology [40]. Concurrently, recent research trends highlight the growing integration of theoretical and computational methods—such as density functional theory (DFT), molecular dynamics (MD), and Monte Carlo (MC) simulations—to complement experimental investigations. These techniques provide valuable insights into molecular reactivity, adsorption behavior, and electrochemical processes occurring at the metal/electrolyte interface [41-46].

In the present study, waterborne copolymers of methyl methacrylate (MMA) and butyl acrylate (BuA) were synthesized at varying monomer ratios via miniemulsion polymerization. The morphology and particle size of the resulting acrylic copolymer nanoparticles were examined using transmission electron microscopy (TEM). At the same time, dynamic light scattering (DLS) was employed to determine the particle size distribution. Although acrylic-based polymers have previously been investigated as corrosion inhibitors, the systematic effect of MMA/BuA copolymer composition on corrosion protection behavior remains insufficiently explored. Therefore, the corrosion inhibition performance of MMA, BuA, and their copolymer emulsions with varying monomer ratios was systematically evaluated in acidic media using electrochemical impedance spectroscopy (EIS) and potentiodynamic polarization (PDP). Particular emphasis was placed on investigating the relationship between the initial MMA/BuA feed ratio, interfacial interactions, and corrosion inhibition behavior. Furthermore, quantum chemical calculations and molecular simulations were conducted to investigate the electronic properties, reactivity, and adsorption characteristics of the polymer nanoparticles at the metal/electrolyte interface, thereby providing a comprehensive experimental–theoretical understanding of their corrosion inhibition mechanism.

2. Experimental

2.1. Materials and sample preparation

Carbon steel specimens were prepared from rods. Before electrochemical measurements, the samples were mechanically abraded using silicon carbide (SiC) emery papers with progressively finer grit sizes ranging from 120 to 2000. The abraded specimens were subsequently rinsed with distilled water, degreased with ethanol, and dried under a stream of hot air. The corrosive medium was a 1 M HCl solution prepared by diluting reagent-grade hydrochloric acid (37%, MERCK, Art. 317) with

Table 1. Chemical composition of the carbon steel specimen

Elements	C	Mn	Si	Cu	Pb	Cr	Ni	Mo	S	B
wt. %	0.16	0.68	0.25	0.2	0.15	0.02	0.05	0.015	0.002	0.0004

distilled water. The exposed surface area of the working electrode in contact with the acidic solution was maintained at 0.78 cm^2. The chemical composition of the carbon steel specimen is presented in Table 1.

2.2. Synthesis of MMA-co-BuA copolymer

The MMA-co-BuA copolymers were synthesized by the miniemulsion polymerization method using different initial monomer feed ratios as illustrated in Figure 1. According to their molecular structures, which are shown in Figure 2, the initial MMA/BuA feed ratios were varied as 80:20, 70:30, 50:50, 30:70, and 20:80 wt% of methyl methacrylate/butyl acrylate. The concentration of total monomers was maintained at 70 wt% in distilled water. In a typical miniemulsion polymerization process, the monomer mixture containing MMA and BuA at the desired feed ratio was prepared as the dispersed organic phase. In contrast, the aqueous phase was prepared separately from distilled water and the required stabilizing components. The monomer phase was then gradually added to the aqueous phase under continuous mixing to form a pre-emulsion. Subsequently, the pre-emulsion was subjected to high-energy dispersion to generate stable nanosized monomer droplets. The polymerization reaction was initiated via a free-radical mechanism, with the monomer droplets serving as nanoreactors for the copolymerization of MMA and BuA, yielding MMA-co-BuA copolymer nanoparticles. The synthesized copolymers were characterized using various techniques, and DLS was used to measure the average particle size of the copolymer nanoparticles. According to the molecular structures of MMA and BuA shown in Figure 2, these monomers exhibit different chemical polarities due to their distinct functional groups and side-chain structures. Therefore, variations in the initial MMA/BuA feed ratio are expected to influence the physicochemical properties and interfacial behavior of the resulting copolymers.

2.3. Measurements

Electrochemical impedance spectroscopy and potentiodynamic polarization were studied using glass electrolytic cells and electrochemical instruments. The glass cell consists of a conventional three-electrode cell, with carbon steel (0.72 cm exposed area) as the working electrode, a platinum wire as the counter electrode, and a saturated calomel electrode as the reference electrode. All electrochemical measurements were performed using an IVIUM Potentiostat (IVIUM Technologies, Fernandina Beach, FL, USA) at room temperature. The working electrode was immersed in the 1 M HCl solution for 20 minutes before EIS and PDP measurements were begun to obtain the steady-state

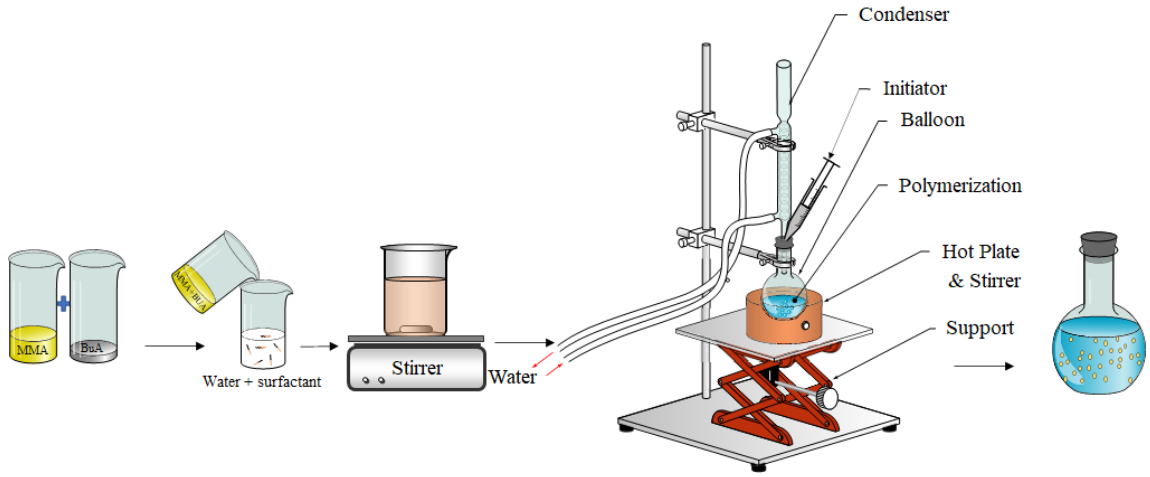

Figure 1. A schematic of the miniemulsion polymerization process.

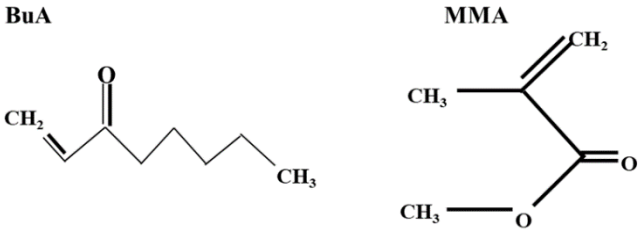

Figure 2. Molecular structures of butyl acrylate and methyl methacrylate.

open-circuit potential (OCP). EIS measurements were conducted at OCP using AC signals with a peak-to-peak amplitude of 10 mV at the frequency range from 100 kHz to 0.01 Hz. The potential was scanned from -250 to +250 mV (vs. OCP) at 1 mV s-1 in both the cathodic and anodic directions.

CM120 Transmission Electron Microscope (TEM) was used to obtain information about the size and morphology of acrylic polymer particles. The Dynamic Light Scattering (DLS) technique was also used to determine the particle size distribution in the polymer latex. Thermal properties of the 20-30 mg N2-dried samples under an inert gas were analyzed by TGA (TGAQ50, TA Instruments) at a heating rate of 10 ◦C/min. The recorded temperature ranged from 20 ˚C to 700 ˚C. Fourier transform infrared spectroscopy (FTIR) analysis was performed to investigate the chemical structure and confirm the successful synthesis of MMA-co-BuA copolymers. The FTIR spectra were recorded using a PerkinElmer Spectrum Two FTIR spectrometer over the wavenumber range of 4000–500 cm^{-1}, and the characteristic absorption bands corresponding to the functional groups of MMA and BuA units were analyzed.

2.4. Theoretical methodology

In the past few years, DFT and MC simulations have drawn scientists' attention as cost- and time-effective tools for predicting corrosion inhibition in metallic materials. In the present work, we used Materials Studio (Accelrys Inc.) software for performing all computational calculations. The Dmol3 module was used for electronic interaction calculations and the geometry optimization of all components, using the Generalized Gradient Approximation (GGA) with the PBE functional and a double numerical quality (DNP) basis set [47, 48]. Critical parameters such as HOMO (Highest Occupied Molecular Orbital) and LUMO (Lowest Unoccupied Molecular Orbital) energies and the energy gap (E) between HOMO and LUMO were also defined.

Monte Carlo simulations were conducted to investigate the adsorption configuration of MMA-BuA copolymer inhibitors on the carbon steel surface. The Fe (110) plane was chosen as the target plane for MC simulations since it exhibits a close-packed structure and is more stable than other Fe planes [49, 50]. Initially, the Fe crystal was imported from the Materials Studio database. After relaxation with the geometry optimization module, the structure was cleaved along the (110) plane. Following that, a simulation vacuum box with constant periodic boundary conditions was built, containing 200 water molecules, 5 H^+ ions, 5 Cl^- ions, and different compositions of the MMA-BuA copolymer inhibitors, to serve as a reliable representative of our corrosive environment. COMPASS (Condensed-phase Optimized Molecular Potentials for Atomistic Simulation Studies) force fields were assigned to all adsorption simulations in the adsorption locator [51].

3. Results and discussion

3.1. Morphological and Particle Size Characterization of MMA–co–BuA Copolymer Nanoparticles

The morphology and particle size of a representative MMA–co–BuA copolymer nanoparticle sample were investigated using transmission electron microscopy (TEM). TEM images of the selected copolymer sample at different magnifications are presented in Figure 3. As observed, the nanoparticles exhibit a relatively spherical morphology with an average particle size of approximately 50 nm. The formation of nanosized particles indicates the successful preparation of the copolymer latex via miniemulsion polymerization.

The particle size characteristics of the selected copolymer latex were further evaluated by dynamic light scattering (DLS). The intensity autocorrelation curve and the corresponding particle size distribution obtained from the DLS analysis are presented in Figure 4. The average hydrodynamic particle size of MMA-co-BuA copolymer nanoparticles measured by DLS was in the range of 40–50 nm, which was comparable to the particle size observed in TEM images.

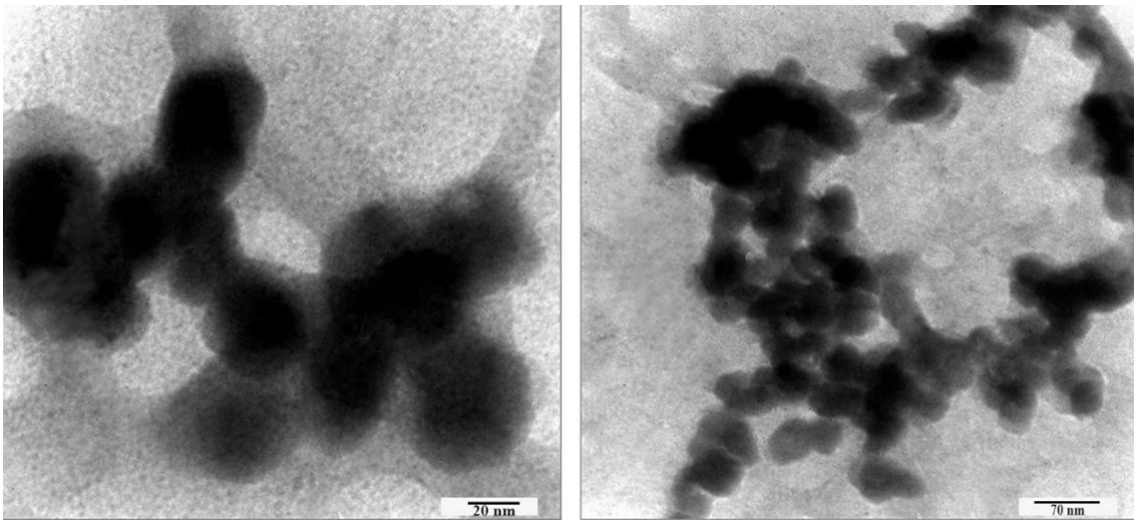

Figure 3. TEM images of MMA-co-BuA copolymer latex at different magnifications.

The slight difference between the particle sizes measured by TEM and DLS can be attributed to the different measurement principles of these techniques. TEM provides the size of dried nanoparticles, whereas DLS determines the hydrodynamic diameter of nanoparticles dispersed in an aqueous medium, including contributions from the surrounding solvent layer. The consistency between TEM and DLS results confirms the formation of nanosized MMA–co–BuA copolymer particles in the investigated sample.

3.2. Fourier Transform Infrared Spectroscopy (FTIR) Analysis

FTIR spectroscopy was employed to investigate the chemical structure of the synthesized MMA-co-BuA copolymer nanoparticles and to provide evidence for the successful formation of the acrylic copolymer structure. Figure 5 presents the FTIR spectra of the MMA-co-BuA copolymers with MMA/BuA ratios of 50/50, 70/30, and 80/20. The spectra exhibit several characteristic absorption bands associated with the functional groups present in the copolymer structure. A broad absorption band observed at approximately 3352–3364 cm^{-1} can be attributed to O–H stretching vibrations, which may mainly originate from adsorbed moisture associated with the aqueous polymeric system. The absorption bands located at approximately 2953–2963 cm^{-1} are assigned to the stretching vibrations of aliphatic C–H bonds in CH_2 and CH_3 groups. A prominent band at 1735 cm^{-1} is observed for all three copolymer compositions. It is attributed to the stretching vibration of the ester carbonyl

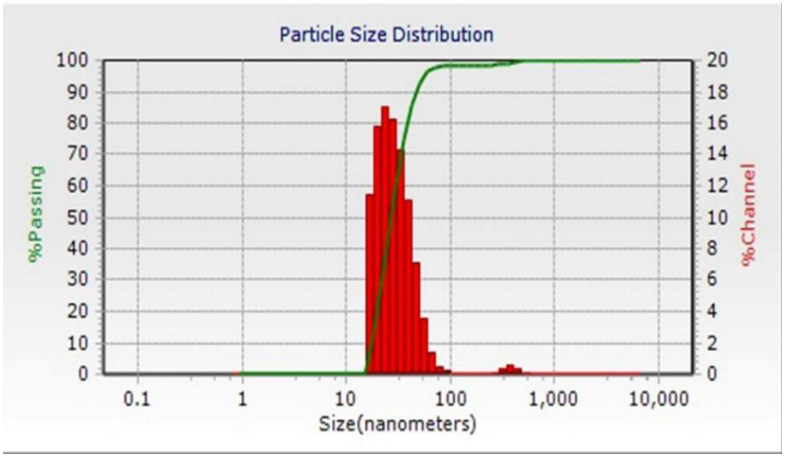

Figure 4. Particle size and the distribution of MMA-co-BuA copolymers by DLS.

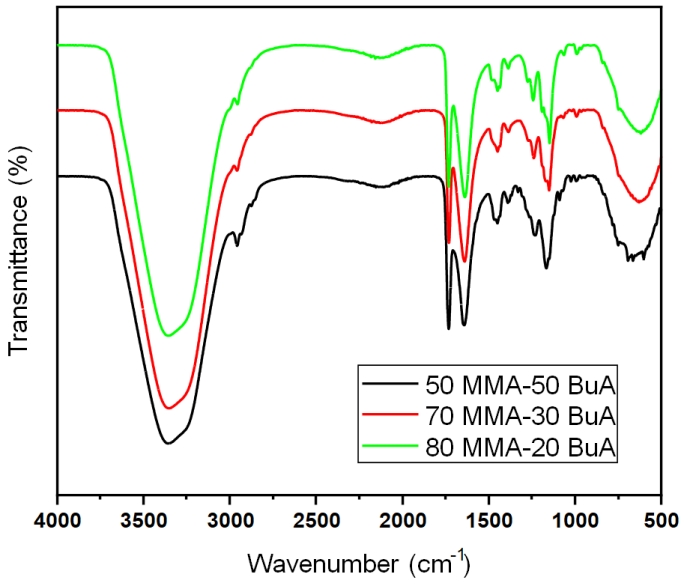

Figure 5. FTIR spectra of MMA-co-BuA copolymer nanoparticles with different MMA/BuA compositions.

(C=O) groups originating from the acrylate and methacrylate units [52]. The bands observed at approximately 1439–1452 cm^{-1} and 1379–1392 cm^{-1} are assigned to bending vibrations of CH_2 and CH_3 groups, respectively [52, 53].

Furthermore, the absorption bands in the range of 1156–1274 cm^{-1} are associated mainly with C–O and C–O–C stretching vibrations of the ester groups [53]. The presence of these characteristic bands in all investigated compositions confirms the presence of the expected functional groups of the MMA- and BuA-derived polymer chains. Although the overall spectral features remain similar for the different compositions, variations in the intensity and position of several bands are observed as the MMA/BuA ratio changes, reflecting differences in the relative contribution of the two monomer units to the copolymer structure. Overall, the FTIR results provide complementary spectroscopic evidence supporting the successful synthesis of the MMA-co-BuA copolymers used in the subsequent morphological, thermal, and electrochemical investigations.

3.3. Thermal Gravimetric Analysis

TGA was used to analyze the thermal stability of the MMA-co-BuA copolymers prepared with different initial MMA/BuA feed ratios. Figure 6 shows the TGA thermograms of the copolymers of MMA and BuA in various compositions (20/80, 30/70, 50/50, 70/30, and 80/20 of MMA/BuA). Table 2 clearly shows that the initiation temperature for the thermal decomposition of the copolymers decreases as the MMA weight percentage increases from 20 to 80. The higher thermal stability in the 80/20 MMA-BuA copolymer may be due to the effect of two carbonyl groups in the molecular structure of MMA polymers.

The 20/80 MMA–BuA copolymer exhibited a slightly different thermal degradation behavior compared with the other compositions. In this sample, a more pronounced weight loss was observed below 400 °C, followed by a slower degradation region between approximately 400 and 500 °C. This behavior may be associated with the higher BuA content, which introduces more flexible alkyl side chains into the copolymer structure and can influence chain mobility and thermal decomposition behavior. However, the overall degradation profile confirms the thermal stability of the synthesized copolymers over a broad temperature range.

3.4. Electrochemical impedance spectroscopy (EIS)

After morphological characterization and thermal gravimetric analysis, electrochemical measurements were performed to evaluate the anti-corrosion performance of the inhibitors. For comparison, EIS measurements were performed to assess the corrosion-inhibition efficiency of

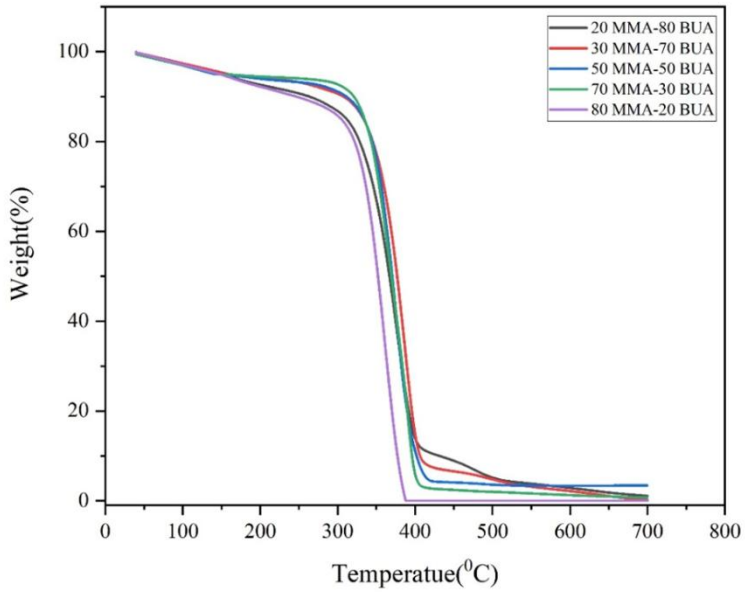

Figure 6. Thermal gravimetric analysis of MMA-co-BuA nanoparticles with different compositions.

MMA-co-BuA copolymers on the carbon steel surface in 1 M HCl solution, in the absence and presence of the inhibitors. Figure 7 represents the Nyquist plots obtained from EIS results of carbon steel in 1 M HCl solution in the absence and presence of copolymer inhibitors. It is noteworthy that with the further addition of MMA-co-BuA copolymers to the acidic media, the impedance response of the working electrode (carbon steel) is liable to change [16]. Additionally, the impedance response has changed following the addition of acrylic compounds as corrosion inhibitors, boosting the metal surface's protection and lowering the metal dissolution rate in an acidic environment. Increasing the MMA fraction in the initial monomer feed ratio increases the diameter of the semicircular arc (Rct), indicating enhanced polarization resistance and reduced corrosion rate. This improvement can be associated with changes in copolymer composition and, in turn, with changes in interfacial interactions between polymer chains and the carbon steel surface. The higher MMA content may contribute to the formation of a more effective adsorbed polymeric layer, which acts as a barrier against the penetration of aggressive species from the acidic electrolyte. Consequently, the corrosion inhibition performance increases with increasing MMA fraction in the initial monomer feed. It reaches its maximum value for the sample synthesized using an 80/20 MMA/BuA feed ratio at a concentration of 40 ppm. The extracted electrochemical parameters obtained from the metal/electrolyte interface are presented in Table 3.

Figure 8 depicts the impedance spectra obtained in the frequency range from 100 kHz to 0.01 Hz for carbon steel in 1 M HCl medium in the presence of poly(MMA-co-BuA) at various concentrations. Clearly, the addition of this copolymer, with varying compositions and concentrations, alters the impedance response of the carbon steel electrode. Figure 7 illustrates the appropriate equivalent circuit, which was determined using EIS analyzer software to quantify and present impedance parameters.

Table 2. Decomposition temperature of MMA-co-BuA copolymers

Inhibitors	Decomposition temperature	Final temperature
80/20 MMA-BuA	147	388
70/30 MMA-BuA	149	416
50/50 MMA-BuA	250	427
30/70 MMA-BuA	235	544
20/80 MMA-BuA	235	548

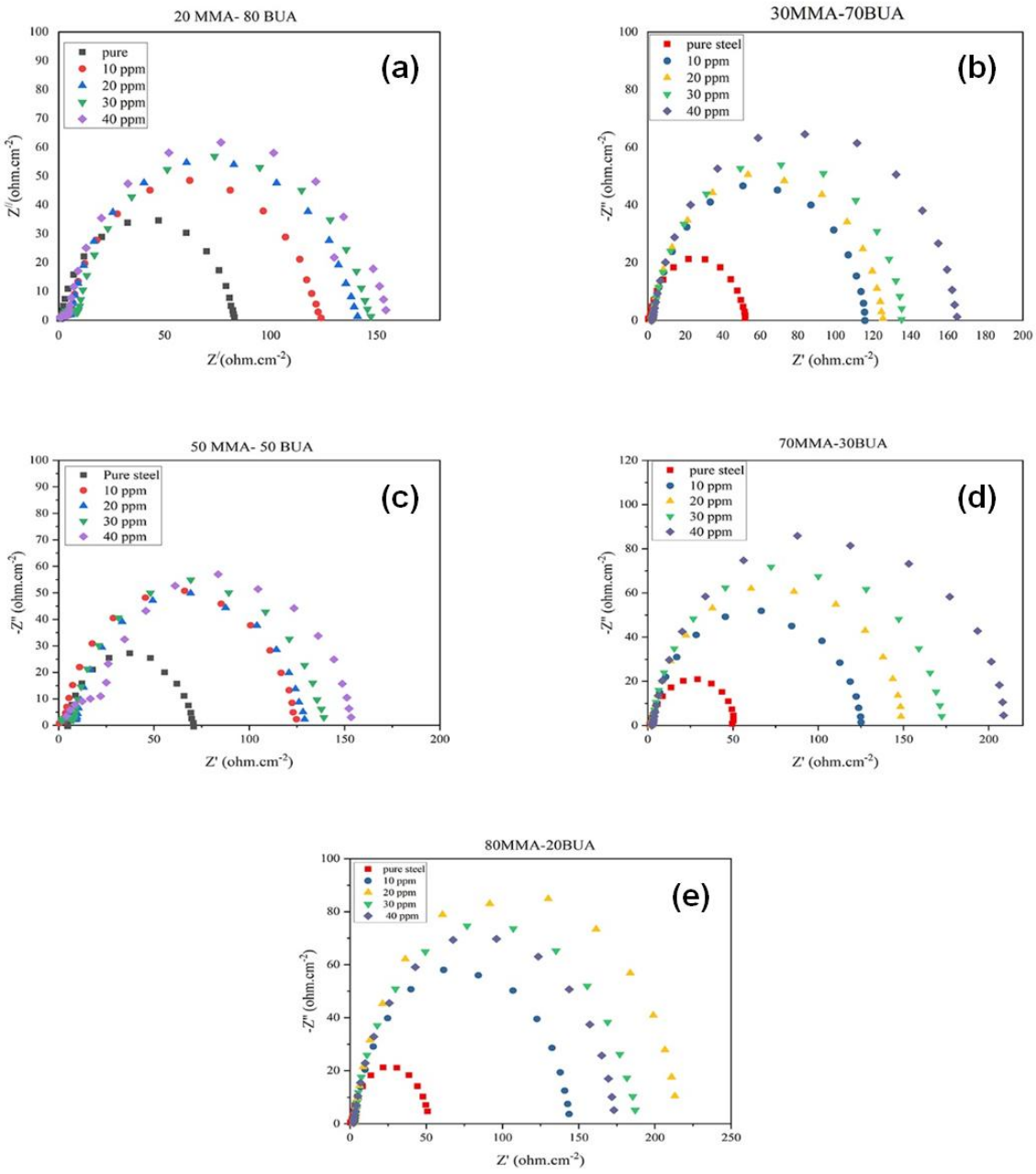

Figure 7. Nyquist plots for carbon steel in the absence and presence of copolymers with various monomer compositions at different concentrations in 1 M HCl solution.

Also, the efficiency of the inhibitors has been calculated from the following equation (1):

$$\%\eta = \frac{R_{ct} - R^0_{ct}}{R_{ct}} \times 100 \qquad (1)$$

where R_{ct} and R^0_{ct} are the charge transfer resistances of the solution with and without the presence of the inhibitors, respectively. The value of R_{ct} was estimated from the diameter of the first high-frequency capacitive loop, and the double-layer capacitance values (C_{dl}) at various inhibitor concentrations are calculated based on the following relationship [15]:

$$C_{dl} = \frac{1}{\omega R_t} = \frac{1}{2\pi f_m R_t} \qquad (2)$$

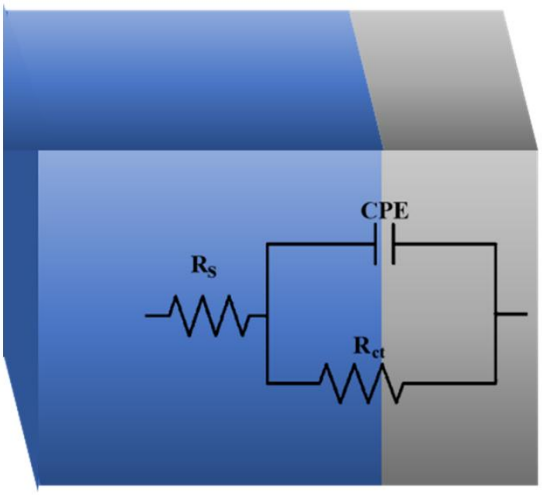

Figure 8. A schematic of an equivalent electrical circuit used to fit EIS results.

where ω is the angular frequency, and f_m is the frequency at the apex of the first capacitive loop.

As a result of micro-roughness and other heterogeneities at the electrode/solution interface during degradation, the loops are naturally depressed, with the center below the X-axis [54]. Additionally, this suggests that electrochemical interactions are controlled by the charge-transfer process [55]. At low frequencies (μF), the recorded capacitive loop may exhibit characteristics of diffusion impedance, which, at maximum copolymer concentrations, transforms into a linear part that characterizes purely capacitive behavior caused by the charge saturation limit set by the finite copolymer thickness adsorbed at the metal/solution interface.

The impedance parameters, such as Rct, Cdl, Re, and θ (surface coverage), obtained from the Nyquist curves are given in Table 3. Increasing the concentration of (MMA-co-BuA) inhibitors in solution results in a higher charge transfer resistance. Moreover, increasing the copolymer concentration decreases the Cdl values. This is due to a reduction in the dielectric constant and/or an increase in the thickness of the electrical double layer. In addition, water molecules at the metal/electrolyte interface are replaced with copolymer molecules. These results suggest

Table 3. Electrochemical data extracted from EIS for carbon steel in 1 M HCl solution in the absence and presence of various concentrations and ratios of MMA-co-BuA copolymers

inhibitors	concentration	Rs (Ω.cm2)	CPEdl (μf.cm-2)	Rct (Ω.cm2)	θ	η (%)
MMA-BuA 80-20	Blank	1.1	390	50.94	-	-
	10	2.84	152	141.7	0.64	64.05
	20	2.42	137	171.8	0.70	70.35
	30	2.54	115	183.9	0.72	72.30
	40	2.88	139	210.8	0.76	75.83
MMA-BuA 70-30	Blank	1.63	474	50.33	-	
	10	2.69	125	121.7	0.59	58.64
	20	2.64	137	146.5	0.66	65.65
	30	2.35	122	169.8	0.70	70.36
	40	2.66	109	207.6	0.76	75.76
MMA-BuA 50-50	Blank	1.15	151	62.79	-	-
	10	5.08	165	118.4	0.47	46.97
	20	5.09	201	135.2	0.54	53.56
	30	8.39	148	138.8	0.55	54.76
	40	4.06	190	151.1	0.58	58.44
MMA-BuA 70-30	Blank	4.65	170	65.24	-	-
	10	2.22	180	120.9	0.46	46.04
	20	8.3	166	123.9	0.47	47.34
	30	7.07	167	132.1	0.51	50.61
	40	7.1	273	138.2	0.53	52.79
MMA-BuA 20-80	Blank	1.05	176	82.32	-	-
	10	2.19	271	119.8	0.31	31.29
	20	2.32	208	120.6	0.32	31.74
	30	2.38	219	124	0.34	33.61
	40	2.34	216	142	0.42	42.03

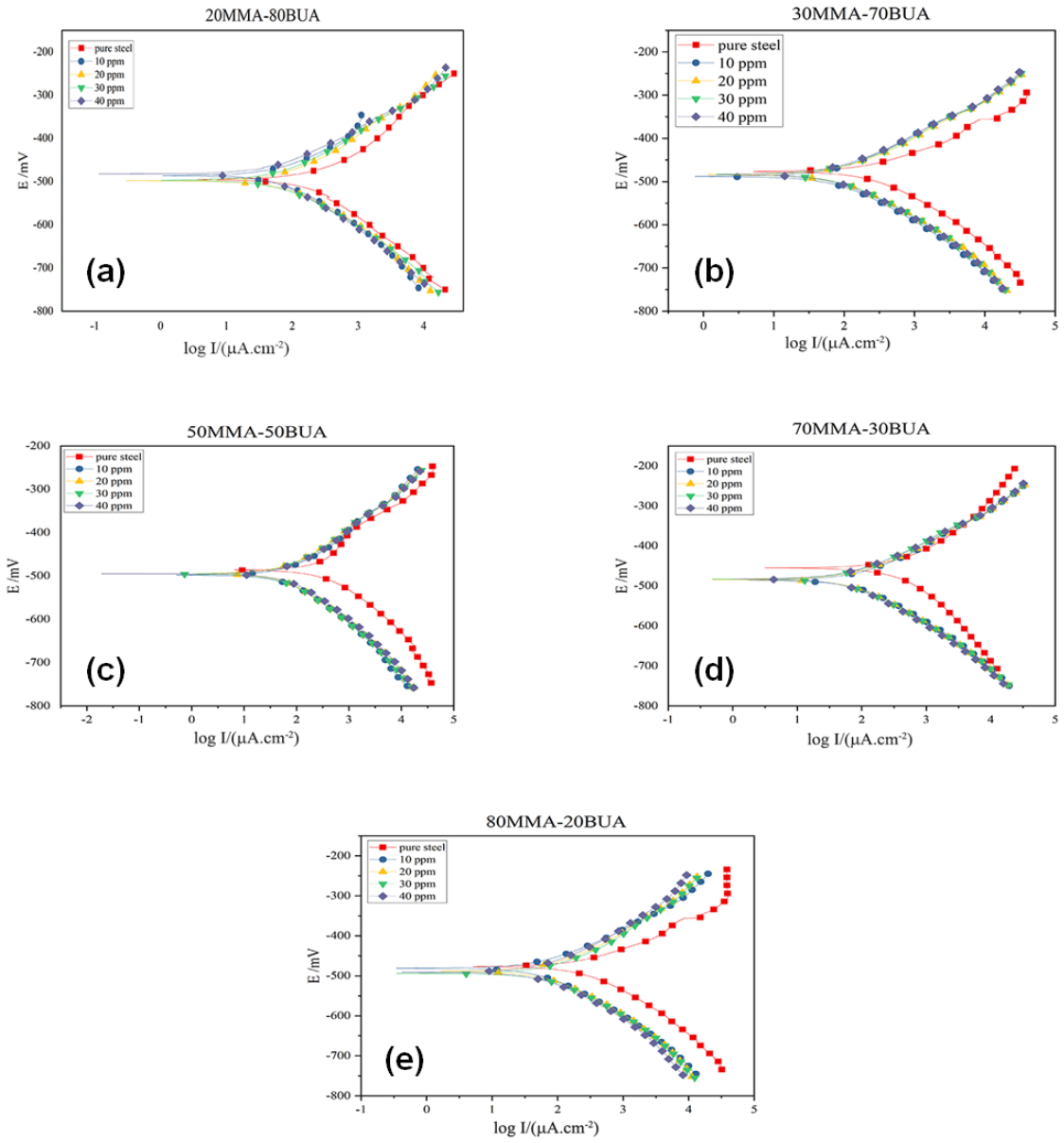

Figure 9. PDP curves for carbon steel in the absence and presence of MMA-co-BuA copolymers with different compositions in 1 M HCl solution.

that copolymer molecules can adsorb onto the carbon steel surface, contributing to the formation of a protective interfacial layer.

The enhanced impedance response in the presence of MMA–co–BuA copolymers can be attributed to the adsorption of polymer chains at the carbon steel/electrolyte interface and the formation of a protective barrier film. The ester functional groups in the copolymer structure contain oxygen atoms with available electron pairs, which can interact with the metal surface via adsorption. This adsorbed polymer layer reduces direct contact between the steel surface and aggressive species, such as H^+ and Cl^- ions, thereby decreasing anodic iron dissolution and cathodic hydrogen evolution. Consequently, the increase in Rct and decrease in Cdl values confirm the formation of a more compact and protective interfacial layer.

The surface coverage of different inhibitor compositions and concentrations in an acidic solution has been analyzed using the following equation [56]:

$$\theta = (1 - \frac{C'_{dl}}{C_{dl}}) \quad (3)$$

Increasing the copolymer concentration in the solution also results in a surge in surface coverage. Nevertheless, the surface coverage reached a maximum with the 80/20 MMA-co-BuA inhibitor, indicating its ability to form a uniform, compact layer on the carbon steel electrode.

3.5. Potentiodynamic polarization measurements (PDP)

From the earlier illustration, the highest corrosion inhibition was achieved by adding 40 ppm of MMA-co-BuA 80-20 copolymer to the solution. To validate the EIS results, we conducted PDP measurements for the copolymer inhibitors at different concentrations. The polarization curves for carbon steel in 1.0 M HCl solution in the absence and presence of different copolymer concentrations are depicted in Figure 9. The electrochemical parameters, including corrosion potential (E_{corr}), corrosion current density (i_{corr}), and cathodic and anodic Tafel slopes (b_a and b_c), were obtained by extrapolating the Tafel slopes [57] are calculated from the polarization curves and listed in Table 4.

It is noteworthy that the following equation is used to calculate the inhibition efficiency of the inhibitors:

$$\eta\% = \frac{i^0_{corr} - i_{corr}}{i^0_{corr}} \times 100 \quad (4)$$

where i^0_{corr} and i_{corr} are corrosion current density values in the absence and presence of the inhibitor, respectively. The polarization resistance values were calculated using Eq. (5) [58].

$$R_p = \frac{b_a \times b_c}{2.303 i_{corr}(b_a + b_c)} \quad (5)$$

where b_a and b_c are anodic and cathodic Tafel slopes, respectively. The effect of the inhibitor concentration of acrylic copolymer on the carbon steel corrosion rate in 1 M HCl solution at 298 K was studied by potentiodynamic polarization and EIS methods.

Table 4. The corrosion rate and efficiency extracted by the PDP test from MMA-co-BuA copolymers in various compositions

inhibitors	Concentration	Ecorr(mV)	icorr (μA/cm2)	ba (mV)	-bc (mV)	CR(mpy)	θ	IE (%)
MMA-BuA 80-20	Blank	-474	12.2	83	122	5.583	-	-
	10	-484	2.81	102	120	1.286	0.770	76.967
	20	-490	2.72	106	119	1.245	0.777	77.705
	30	-477	2.28	83	110	1.043	0.813	81.311
	40	-485	2.11	106	123	0.966	0.827	82.705
MMA-BuA 70-30	Blank	-456	12.3	102	132	5.629	-	-
	10	-487	3.25	82	86	1.487	0.736	73.577
	20	-485	3.02	74	84	1.382	0.754	75.447
	30	-480	2.68	68	84	1.226	0.782	78.211
	40	-482	2.53	63	84	1.158	0.794	79.431
MMA-BuA 50-50	Blank	-484	12.01	120	82	5.496	-	-
	10	-498	3.09	70	80	1.414	0.743	74.271
	20	-494	3.06	72	80	1.400	0.745	74.521
	30	-493	2.79	71	84	1.277	0.768	76.769
	40	-493	2.76	68	79	1.263	0.770	77.019
MMA-BuA 70-30	Blank	-473	11.6	83	122	5.309	-	-
	10	-484	4.58	70	90	2.096	0.605	60.517
	20	-482	4.29	68	86	1.963	0.630	63.017
	30	-483	3.87	70	84	1.771	0.666	66.638
	40	-482	3.02	70	80	1.382	0.740	73.966
MMA-BuA 20-80	Blank	-523	11.5	81	99	5.263	-	-
	10	-586	3.69	68	80	1.689	0.679	67.913
	20	-499	3.58	85	82	1.638	0.689	68.870
	30	-493	3.17	73	79	1.451	0.724	72.435
	40	-481	3.16	69	87	1.446	0.725	72.522

According to Figure 9 and Table 4, the addition of MMA–co–BuA copolymer inhibitors significantly decreases both anodic and cathodic current densities, confirming their effective role in reducing the corrosion rate of carbon steel in 1 M HCl solution Among the investigated samples, the 80/20 MMA–BuA copolymer at a concentration of 40 ppm exhibited the lowest corrosion current density (2.11 μA cm^{-2}) and the highest inhibition efficiency (82.7%), which is in good agreement with the EIS results. In addition, they hinder the hydrogen evolution reaction at the metal/electrolyte interface by adsorbing on the metal surface with their long carbon chains [59-61].

The changes observed in both anodic and cathodic Tafel slopes after the addition of copolymer inhibitors indicate that the polymer molecules influence both electrochemical reactions occurring at the metal/electrolyte interface. Furthermore, the relatively limited variation in Ecorr values suggests that the synthesized copolymers do not selectively suppress only one electrochemical reaction. Therefore, MMA–co–BuA copolymers can be considered mixed-type inhibitors that mainly act through adsorption onto the carbon steel surface. The corrosion inhibition mechanism can be attributed to the adsorption of polymer chains and the formation of a protective interfacial film. The ester functional groups in the MMA–co–BuA copolymer structure provide electron-rich oxygen atoms that can interact with the metal surface, promoting the formation of an adsorbed polymer layer. This protective layer reduces direct contact between the steel surface and aggressive ions, thereby reducing both anodic iron dissolution and cathodic hydrogen evolution. The increase in inhibition efficiency with increasing copolymer concentration can be related to the greater availability of polymer molecules for adsorption and improved surface coverage. In addition, variations in the initial MMA/BuA feed ratio influence the physicochemical characteristics of the resulting copolymer chains and their interactions with the metal/electrolyte interface, thereby affecting protection performance. The higher efficiency observed for the 80/20 MMA–BuA copolymer can therefore be associated with the formation of a more effective protective layer on the carbon steel surface.

3.6. Quantum Chemical Calculations

DFT has been widely recognized as an accurate method for determining fundamental molecular parameters, regardless of molecular complexity [62, 63]. This study demonstrates a relationship between molecular quantum parameters and experimental data obtained from electrochemical measurements of five copolymer inhibitors on carbon steel in 1 M HCl solution. Based on molecular frontier orbital theory, HOMO and LUMO are reliable factors representing the tendency of the inhibitor molecule to interact with the metal surface. The energy gap between HOMO and LUMO energies is of paramount importance in describing absorption characteristics. Accordingly, higher values of HOMO energy are an indication of the ability to supply electrons via its outer orbital layer to electron-deficient centers. In comparison, lower LUMO energies indicate the ability of the inhibitors to accept electrons from the vacant orbitals of metal atoms. Therefore, lower energy gaps indicate more robust inhibition efficiency [64, 65].

The distribution of the frontier molecular orbitals for each polymer is illustrated in Figure 10. As can be seen, the HOMO is distributed almost around the entire MMA molecule, and the LUMO is focused at the molecule's center adjacent to the oxygen atoms, particularly around the C=C bond in the ($CH = CH_2$) vinyl group in the MMA molecule. Consequently, the MMA molecule has a much greater propensity to donate its unpaired electrons to unoccupied molecular orbitals of the metal surface than BuA. Hence, increasing the MMA fraction in the initial monomer feed is associated with enhanced inhibition efficiency. By scrutinizing the LUMO distribution, it can be observed that it is centered on the carbon and hydrogen atoms of the MMA molecule and the oxygen atoms of the BuA molecule. This means that these atoms are responsible for accepting electrons while the inhibitor is interacting with the metal surface. Quantum-chemical parameters, including HOMO and LUMO energies and the Egap energy, are listed in Table 5. MMA shows higher E_{HOMO} and lower E_{LUMO}. Thus, the energy gap for the

Table 5. DFT data calculated from the chemical parameters of monomers

Monomers	EHOMO (eV)	ELUMO (eV)	ΔE (eV)
Methyl methacrylate	-5.579	-2.764	2.815
Butyl acrylate	-6.315	-2.283	4.032

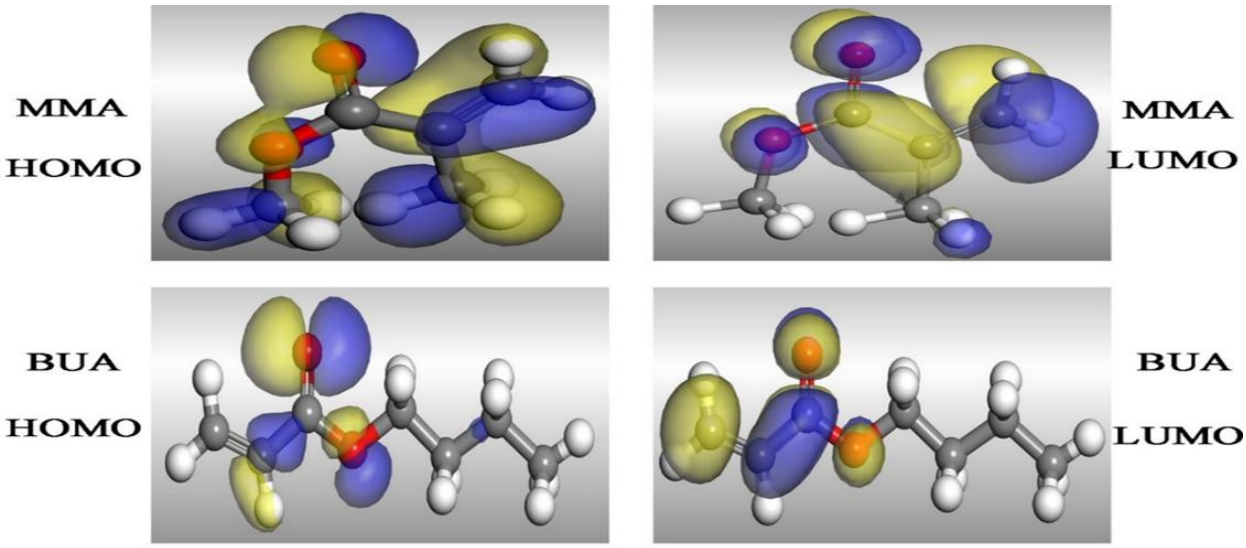

Figure 10. HOMO/LUMO distribution for MMA and BuA molecules obtained from DFT calculations.

MMA monomer is significantly less than that of BuA, meaning that it has much more acceptable anticorrosive characteristics. According to the above analysis, our quantum chemical calculations for both inhibitors are consistent with the electrochemical measurements.

3.7. Monte Carlo Simulation (MC)

From atomic-scale MC simulations, we obtain valuable insights into the orientation and adsorption configuration of corrosion inhibitors at metal-electrolyte interfaces, enabling the development of novel high-performance corrosion inhibitors [66, 67]. The adsorption of the MMA-co-BuA copolymers with different compositions on the metal surface was theoretically simulated by MC, and the side views of the simulation cell are shown in Figure 11. Comparing the snapshots obtained from the atomic-scale simulation, we can deduce that all the copolymer inhibitors are partially adsorbed to the iron (110) surface.

Table 6. The adsorption energies calculated by MC simulations on the Fe (110) surface for the adsorption of MMA-BuA copolymer at 298 K in 1 M HCl solution

Monomers	$E_{adsorption}$ ($\times 10^4$ kcal/mol)
80/20 MMA-BuA	-0.299
70/30 MMA-BuA	-0.292
50/50 MMA-BuA	-0.288
30/70 MMA-BuA	-0.265
20/80 MMA-BuA	-0.257

Detailed analysis of the MMA-BuA 80-20 copolymer reveals that most components are arranged in a parallel configuration adjacent to the metal surface, covering it to a significant extent. Adsorption generally occurs when corrosive ions, such as hydronium and chloride ions, are replaced by inhibitor molecules on the surface of metal specimens. Based on the high negative interaction energies between MMA-co-BuA copolymer inhibitor molecules and the carbon steel surface, it can be concluded that the interaction between inhibitor molecules and the iron surface is spontaneous, robust, and stable [68, 69]. According to Table 6, the final shots of the MC simulation were determined based on the adsorption energies. For comparison, increasing the MMA fraction in the initial monomer feed used for copolymer synthesis resulted in lower adsorption energy, suggesting that the copolymer with an 80-20 MMA/BuA composition would exhibit the highest inhibition performance. Our atomic-scale simulations and quantum-chemical calculations verified our electrochemical results based on the above analysis.

4. Conclusions

A combination of potentiodynamic polarization, electrochemical impedance spectroscopy, density functional theory, and Monte Carlo simulation was used in this study to examine the synergistic effect of a methyl

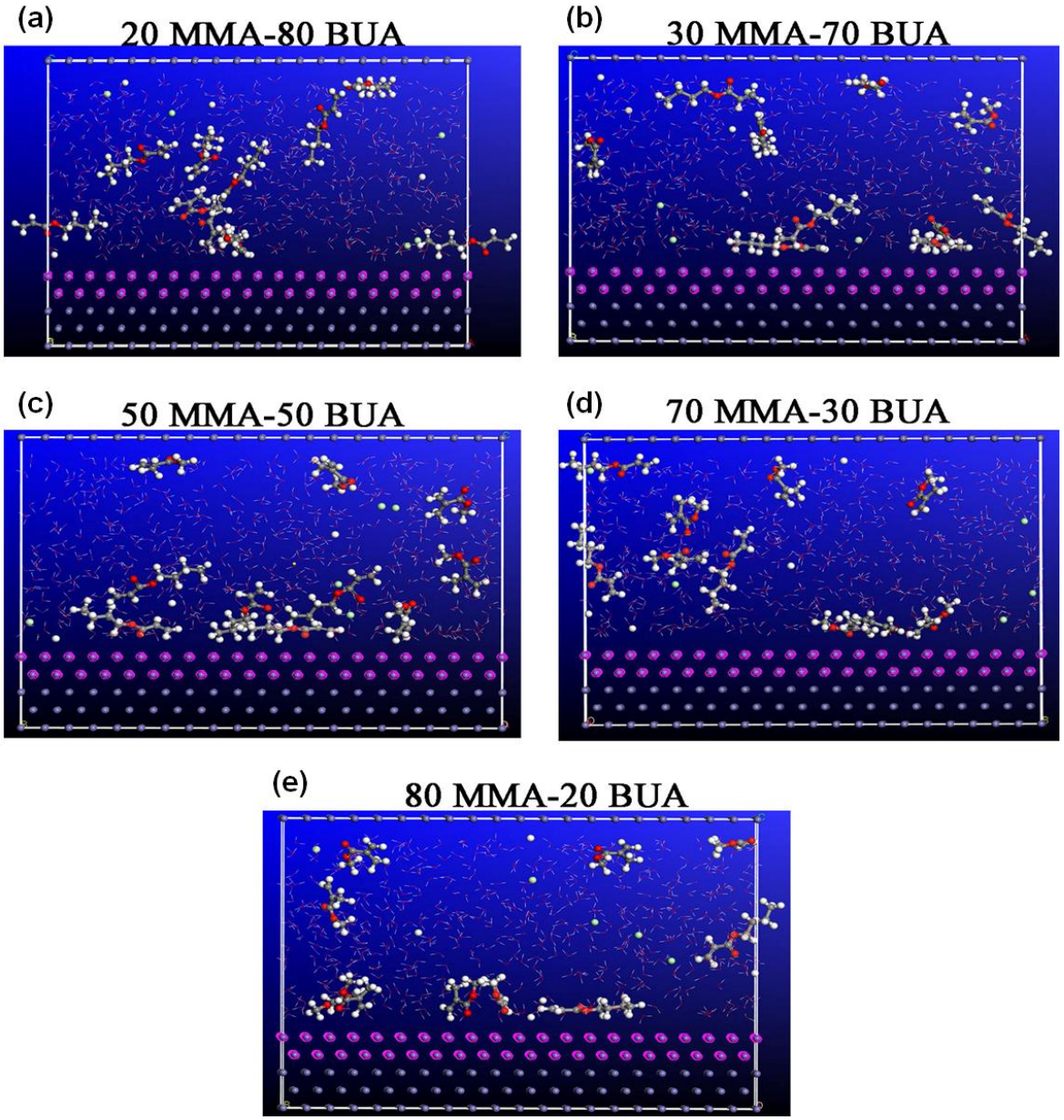

Figure 11. Equilibrium adsorption configuration of copolymer nanoparticles with different compositions on the Fe (110) surface at 298 K in an acidic solution, obtained by MC simulation.

methacrylate-butyl acrylate copolymer as a corrosion inhibitor for carbon steel in 1 M HCl solution at room temperature. Morphology characterization and particle size distribution were carried out using TEM, DLS, and TGA. Experimental data show that mixing corrosion inhibitors, regardless of composition, significantly reduces the rate of carbon steel degradation. When an initial MMA/BuA feed ratio of 4:1 was used for copolymer synthesis, the inhibition performance reached 82.7% at 40 ppm concentration. Theoretical investigations (DFT and MC) were performed on the iron (110) surface. Different compositions of MMA-BuA copolymer nanoparticles can adsorb to the metal surface, forming a condensed barrier film. However, when the MMA to BuA ratio is 4:1, the most extensive surface coverage and the maximum synergistic effect are

achieved in acidic media. Moreover, theoretical results confirmed the superior anti-corrosion performance of the 80/20 MMA-BuA copolymer.

Conflict of Interest

The authors declare no conflict of interest.

References

1. V.S. Sastri, *Corrosion Inhibitors: Principles and Applications*. Shreir's Corrosion. **1998**: Wiley.
2. E.E. Ebenso, D.A. Isabirye, and N.O. Eddy. Adsorption and Quantum Chemical Studies on the Inhibition Potentials of Some Thiosemicarbazides for the Corrosion of Mild Steel in Acidic Medium. *International Journal of Molecular Sciences*, **2010**, *11*, 2473.
3. E.-S.M. Sherif, et al. Electrochemical Studies on the Corrosion Behavior of API X65 Pipeline Steel in Chloride Solutions. *International Journal of Electrochemical Science*, **2013**, *8*, 9360.
4. I.A. Yakubtsov, P. Poruks, and J.D. Boyd. Microstructure and mechanical properties of bainitic low carbon high strength plate steels. *Materials Science and Engineering: A*, **2008**, *480*, 109.
5. M. Ramezanzadeh, et al. Highly effective inhibition of mild steel corrosion in 3.5% NaCl solution by green Nettle leaves extract and synergistic effect of eco-friendly cerium nitrate additive: Experimental, MD simulation and QM investigations. *Journal of Molecular Liquids*, **2018**, *256*, 67.
6. M.S. Baktash, et al. Development and optimization of a new hybrid chitosan-grafted graphene oxide/magnetic nanoparticle system for theranostic applications. *Journal of Molecular Liquids*, **2021**, *322*, 114515.
7. M.A. Migahed, et al. Synthesis and evaluation of a new water soluble corrosion inhibitor from recycled poly(ethylene terphethalate). *Materials Chemistry and Physics*, **2010**, *121*, 208.
8. W. Zhang, Y.-C. Wu, and H.-J. Li. Apostichopus japonicus polysaccharide as efficient sustainable inhibitor for mild steel against hydrochloric acid corrosion. *Journal of Molecular Liquids*, **2021**, *321*, 114923.
9. K. Li, et al. A facile synthesis of graphene oxide/locust bean gum hybrid aerogel for water purification. *Carbohydrate Polymers*, **2021**, *254*, 117318.
10. R. Sahraei and M. Ghaemy. Synthesis of modified gum tragacanth/graphene oxide composite hydrogel for heavy metal ions removal and preparation of silver nanocomposite for antibacterial activity. *Carbohydrate Polymers*, **2017**, *157*, 823.
11. A. Saady, et al. Chemical, electrochemical, quantum, and surface analysis evaluation on the inhibition performance of novel imidazo[4,5-b] pyridine derivatives against mild steel corrosion. *Corrosion Science*, **2021**, *189*, 109621.
12. Z. Wetwet. Investigation of Wear Resistance and Corrosion of Ni-PTFE Composite Coatings Prepared by Electrodeposition Method. *Journal of Applied Material Science*, **2025**, *1*, e210148.
13. S. Shiri. Comparison of the Corrosion Inhibition Effect of Portulaca oleracea Extracts Prepared Using Ethanol and Water. *Journal of Applied Material Science*, **2025**, *1*, e210150.
14. S. Shiri. Exploring Corrosion Protection Potential of Sustainable and Green Morus alba 'Pendula' Fruit Extracts. *Journal of Applied Material Science*, **2025**, *1*, e210139.
15. R. Kumar, et al. Corrosion inhibition performance of chromone-3-acrylic acid derivatives for low alloy steel with theoretical modeling and experimental aspects. *Journal of Molecular Liquids*, **2017**, *243*, 439.
16. M. Vakili Azghandi, et al. Water-base acrylic terpolymer as a corrosion inhibitor for SAE1018 in simulated sour petroleum solution in stagnant and hydrodynamic conditions. *Corrosion Science*, **2012**, *64*, 44.
17. T.A. Saleh, et al. Synthesis of Amine Grafted Poly (Acrylic-Maleic) as an efficient inhibitor against stainless steel corrosion in a highly saline medium. *Progress in Organic Coatings*, **2022**, *170*, 106974.
18. E. González, et al. Assessing the Effect of CeO2 Nanoparticles as Corrosion Inhibitor in Hybrid Biobased Waterborne Acrylic Direct to Metal Coating Binders. *Polymers*, **2021**, *13*, 848.
19. M. Mobin, et al. Biopolymer from Tragacanth Gum as a Green Corrosion Inhibitor for Carbon Steel in 1 M HCl Solution. *ACS Omega*, **2017**, *2*, 3997.
20. C. Verma, et al. Aqueous phase environmental friendly organic corrosion inhibitors derived from one step multicomponent reactions: A review. *Journal of Molecular Liquids*, **2019**, *275*, 18.
21. C. Verma, M.A. Quraishi, and K.Y. Rhee. Aqueous phase polymeric corrosion inhibitors: Recent advancements and future opportunities. *Journal of Molecular Liquids*, **2022**, *348*, 118387.
22. K. Landfester. SYNTHESIS OF COLLOIDAL PARTICLES IN MINIEMULSIONS. *Annual Review of Materials Research*, **2006**, *36*, 231.
23. F.J. Schork, et al., *Miniemulsion Polymerization*, in *Advances in Polymer Science*. **2005**, Springer Berlin Heidelberg. p. 129.
24. O.W. Webster, *Group Transfer Polymerization: A Critical Review of Its Mechanism and Comparison with Other Methods for Controlled Polymerization of Acrylic Monomers*, in *Advances in Polymer Science*. **2003**, Springer Berlin Heidelberg.

25. P. Jain, B. Patidar, and J. Bhawsar. Potential of Nanoparticles as a Corrosion Inhibitor: A Review. *Journal of Bio- and Tribo-Corrosion*, **2020**, *6*, 1.

26. X. Wang, et al. Recent Progress of Polymeric Corrosion Inhibitor: Structure and Application. *Materials*, **2023**, *16*, 2954.

27. Y. Liu, et al. Advances in polymer corrosion inhibitors: Mechanisms, challenges, and prospects. *Materials Today Communications*, **2025**, *46*, 112759.

28. F. Yang, et al. Corrosion Inhibition of Polydopamine Nanoparticles on Mild Steel in Hydrochloric Acid Solution. *International Journal of Electrochemical Science*, **2017**, *12*, 7469.

29. T.-C. Huang, et al. Advanced anti-corrosion coatings prepared from α-zirconium phosphate/polyurethane nanocomposites. *RSC Advances*, **2017**, *7*, 9908.

30. S.A. Sajjadi, et al. A comparative study on the effect of type of reinforcement on the scratch behavior of a polyacrylic-based nanocomposite coating. *Journal of Coatings Technology and Research*, **2012**, *10*, 255.

31. M.S. Kumar, et al. Carbon-polyaniline nanocomposites as supercapacitor materials. *Materials Research Express*, **2018**, *5*, 045505.

32. M.I. Khan, et al. Synthesis, Characterization and Application of Ferrochrome slag/polyaniline Nanocomposite as Corrosion Protection Coatings for Carbon Steel. *International Journal of Electrochemical Science*, **2018**, *13*, 7385.

33. S.K. Shukla, M.A. Quraishi, and R. Prakash. A self-doped conducting polymer "polyanthranilic acid": An efficient corrosion inhibitor for mild steel in acidic solution. *Corrosion Science*, **2008**, *50*, 2867.

34. S.A. Umoren and I.B. Obot. POLYVINYLPYROLLIDONE AND POLYACRYLAMIDE AS CORROSION INHIBITORS FOR MILD STEEL IN ACIDIC MEDIUM. *Surface Review and Letters*, **2008**, *15*, 277.

35. G. Cui, et al. Chitosan oligosaccharide derivatives as green corrosion inhibitors for P110 steel in a carbon-dioxide-saturated chloride solution. *Carbohydrate Polymers*, **2019**, *203*, 386.

36. M. Srimathi, R. Rajalakshmi, and S. Subhashini. Polyvinyl alcohol–sulphanilic acid water soluble composite as corrosion inhibitor for mild steel in hydrochloric acid medium. *Arabian Journal of Chemistry*, **2014**, *7*, 647.

37. E. Udabe, et al. Design of Polymeric Corrosion Inhibitors Based on Ionic Coumarate Groups. *ACS Applied Polymer Materials*, **2021**, *3*, 1739.

38. S. Ji, et al. Molecular design and copolymerization to enhance the anti-corrosion performance of waterborne acrylic coatings. *Progress in Organic Coatings*, **2021**, *153*, 106140.

39. T. Chen, et al. Evaluation of anti-corrosion performance of poly(maleic acid-co-N-[3-(dimethylamino)propyl]-methacrylamide) as novel copolymer inhibitor for carbon steel in neutral medium. *Journal of Molecular Liquids*, **2021**, *338*, 116638.

40. C. Wang, et al. Hybrid polymer latexes: acrylics–polyurethane from miniemulsion polymerization: properties of hybrid latexes versus blends. *Polymer*, **2005**, *46*, 1113.

41. N. Cao, et al. Nanopore microspheres prepared by a cationic surfmer in the miniemulsion polymerization of styrene. *Journal of Polymer Science Part A: Polymer Chemistry*, **2007**, *45*, 5800.

42. A. Chaouiki, et al. Exploring deep insights into the interaction mechanism of a quinazoline derivative with mild steel in HCl: electrochemical, DFT, and molecular dynamic simulation studies. *Journal of Adhesion Science and Technology*, **2019**, *33*, 921.

43. R. Hsissou, et al. Anticorrosive property of hexafunctional epoxy polymer HGTMDAE for E24 carbon steel corrosion in 1.0 M HCl: gravimetric, electrochemical, surface morphology and molecular dynamic simulations. *Polymer Bulletin*, **2019**, *77*, 3577.

44. I.B. Obot, D.D. Macdonald, and Z.M. Gasem. Density functional theory (DFT) as a powerful tool for designing new organic corrosion inhibitors. Part 1: An overview. *Corrosion Science*, **2015**, *99*, 1.

45. Z. Salarvand, et al. Enhanced corrosion resistance of mild steel in 1M HCl solution by trace amount of 2-phenyl-benzothiazole derivatives: Experimental, quantum chemical calculations and molecular dynamics (MD) simulation studies. *Corrosion Science*, **2017**, *114*, 133.

46. A. Singh, et al. Effect of electron donating functional groups on corrosion inhibition of mild steel in hydrochloric acid: Experimental and quantum chemical study. *Journal of the Taiwan Institute of Chemical Engineers*, **2018**, *82*, 233.

47. C. Verma, et al. Molecular dynamics and Monte Carlo simulations as powerful tools for study of interfacial adsorption behavior of corrosion inhibitors in aqueous phase: A review. *Journal of Molecular Liquids*, **2018**, *260*, 99.

48. A.D. Becke. A multicenter numerical integration scheme for polyatomic molecules. *The Journal of Chemical Physics*, **1988**, *88*, 2547.

49. C. Lee, W. Yang, and R.G. Parr. Development of the Colle-Salvetti correlation-energy formula into a functional of the electron density. *Physical Review B*, **1988**, *37*, 785.

50. L. Li, et al. The discussion of descriptors for the QSAR model and molecular dynamics simulation of benzimidazole derivatives as corrosion inhibitors. *Corrosion Science*, **2015**, *99*, 76.

51. I.B. Obot, et al. Experimental, quantum chemical calculations, and molecular dynamic simulations insight into the corrosion inhibition properties of 2-(6-methylpyridin-2-yl)oxazolo[5,4-

f][1,10]phenanthroline on mild steel. *Research on Chemical Intermediates*, **2012**, *39*, 1927.

52. S. Gong, et al. Synthesis and applications of MANs/poly(MMA-co-BA) nanocomposite latex by miniemulsion polymerization. *Royal Society Open Science*, **2017**, *4*, 170844.

53. Z. He, et al. Synthesis and Preparation of (Acrylic Copolymer) Ternary System Peelable Sealing Decontamination Material. *Polymers*, **2020**, *12*, 1556.

54. A. Dehghani, G. Bahlakeh, and B. Ramezanzadeh. Construction of a sustainable/controlled-release nano-container of non-toxic corrosion inhibitors for the water-based siliconized film: Estimating the host-guest interactions/desorption of inclusion complexes of cerium acetylacetonate (CeA) with beta-cyclodextrin (β-CD) via detailed electronic/atomic-scale computer modeling and experimental methods. *Journal of Hazardous Materials*, **2020**, *399*, 123046.

55. H. Kato, et al. Accurate Size and Size-Distribution Determination of Polystyrene Latex Nanoparticles in Aqueous Medium Using Dynamic Light Scattering and Asymmetrical Flow Field Flow Fractionation with Multi-Angle Light Scattering. *Nanomaterials*, **2012**, *2*, 15.

56. W. Frankema, et al. Characterisation of core-shell latexes by flow field-flow fractionation with multi-angle light scattering detection. *Journal of Chromatography A*, **2002**, *943*, 251.

57. A.C. Makan, et al. Advanced analysis of polymer emulsions: Particle size and particle size distribution by field-flow fractionation and dynamic light scattering. *Journal of Chromatography A*, **2016**, *1442*, 94.

58. A. Dutta, et al. Effect of substitution on corrosion inhibition properties of 2-(substituted phenyl) benzimidazole derivatives on mild steel in 1 M HCl solution: A combined experimental and theoretical approach. *Corrosion Science*, **2017**, *123*, 256.

59. A. Döner, et al. Experimental and theoretical studies of thiazoles as corrosion inhibitors for mild steel in sulphuric acid solution. *Corrosion Science*, **2011**, *53*, 2902.

60. Y. Yi, et al. The Use of Conducting Polyaniline as Corrosion Inhibitor for Mild Steel in Hydrochloric Acid. *International Journal of Electrochemical Science*, **2013**, *8*, 3540.

61. G. Sığırcık, D. Yildirim, and T. Tüken. Synthesis and inhibitory effect of N,N'-bis(1-phenylethanol)ethylenediamine against steel corrosion in HCl Media. *Corrosion Science*, **2017**, *120*, 184.

62. M. Stern. Closure to "Discussion of 'Electrochemical Polarization, 1. A Theoretical Analysis of the Shape of Polarization Curves' [M. Stern and A. L. Geary (pp. 56–63, Vol. 104)]". *Journal of The Electrochemical Society*, **1957**, *104*, 751.

63. A. Kosari, et al. Electrochemical and quantum chemical assessment of two organic compounds from pyridine derivatives as corrosion inhibitors for mild steel in HCl solution under stagnant condition and hydrodynamic flow. *Corrosion Science*, **2014**, *78*, 138.

64. M.A. Hegazy, et al. Corrosion inhibition of carbon steel using novel N-(2-(2-mercaptoacetoxy)ethyl)-N,N-dimethyl dodecan-1-aminium bromide during acid pickling. *Corrosion Science*, **2013**, *69*, 110.

65. J. Aljourani, K. Raeissi, and M.A. Golozar. Benzimidazole and its derivatives as corrosion inhibitors for mild steel in 1M HCl solution. *Corrosion Science*, **2009**, *51*, 1836.

66. F. Zhang, et al. Performance and theoretical study on corrosion inhibition of 2-(4-pyridyl)-benzimidazole for mild steel in hydrochloric acid. *Corrosion Science*, **2012**, *61*, 1.

67. R. Yıldız. An electrochemical and theoretical evaluation of 4,6-diamino-2-pyrimidinethiol as a corrosion inhibitor for mild steel in HCl solutions. *Corrosion Science*, **2015**, *90*, 544.

68. M.R. Barrodi, et al., *Synergistic Effect in Tragacanth Gum-Ceftriaxone Hybrid System as an Environmentally Friendly Corrosion Inhibitor for Mild Steel in Acidic Solutions*. **2022**, Elsevier BV.

69. M. Talari, et al. Experimental and computational chemistry studies of two imidazole-based compounds as corrosion inhibitors for mild steel in HCl solution. *Journal of Molecular Liquids*, **2019**, *286*, 110915.